Proceedings of the ASME 2014 Conference on Smart Materials, Adaptive Structures and Intelligent Systems
SMASIS2014
September 8-10, 2014, Newport, Rhode Island, USA

SMASIS2014-7710

SMART STRUCTURE INTEGRATION THROUGH ULTRASONIC ADDITIVE MANUFACTURING

Marcelo J. Dapino*
Smart Materials and Structures Laboratory
NSF I/UCRC on Smart Vehicle Concepts
Dept. of Mechanical and Aerospace Engineering
The Ohio State University
Columbus, Ohio 43210
Email: dapino.1@osu.edu

ABSTRACT

Ultrasonic additive manufacturing (UAM), a form of 3D printing based on ultrasonic metal welding, allows for room-temperature fabrication of adaptive structures with seamlessly embedded sensors and actuators. UAM combines solid-state welding of metallic foils, automated additive foil layering, and CNC machining. The most recent UAM systems utilize 9 kW of ultrasonic power for improved build strength and quality over low power systems, leading to previously unfeasible smart structures. Current UAM efforts in this area are focused on embedding smart materials, fiber optics, and cooling channels into metallic matrices. Since UAM process temperatures do not exceed one half of the melting temperature of the matrix, various alloys such as NiTi and FeGa, and polymers such as PVDF, have been successfully embedded without degradation of the smart material or the matrix. This paper aims to demonstrate the benefits of UAM, with particular emphasis on smart components for vehicle design. Example concepts include stiffness-tunable structures, thermally invariant composites, and materials with embedded cooling channels.

1 INTRODUCTION

Worldwide sales of additive manufacturing products and services is estimated to reach $11bn in 2021, up from $2bn in 2012 [1]. Despite this anticipated level of growth, the value of additive manufacturing is unclear, especially for industry sectors that rely on mass manufacturing. As a relatively new technology, additive manufacturing has not yet reached the levels of throughput, cost structure, and standardization required in industry sectors such as automotive and electronics. That being said, additive manufacturing presents a key target of opportunity for creating lightweight multifunctional structures with embedded sensors, actuators, and electronic components. Both fundamental and applied studies are needed in order to address present technical challenges and move additive manufacturing from the laboratory to practical applications.

This paper is focused on ultrasonic additive manufacturing (UAM), a recent form of 3D printing which promises to enable adaptive structures with seamlessly embedded sensors and actuators [2]. UAM combines solid-state ultrasonic welding of metallic foils, automated additive foil layering, and a CNC machining center to create fully dense, gapless metallic components and structures. A key benefit of UAM is low process temperatures, typically less than one half of the melting temperature of the constituent metals. The low thermal loading implies that finished parts suffer no heat induced distortion, and hence no remedial machining is required to bring parts to their intended dimensions. Further, the overall UAM process is energetically efficient as the input stock (foils) require less processing energy than the pellets used in fusion-based additive manufacturing processes. UAM

*Address all correspondence to this author.

structures can have complex external and internal 3D geometries, can be composed of dissimilar metals such as aluminum, titanium, or copper, and can include embedded features such as RF antennas, electronic circuits, fiber optics, smart sensors and actuators, cooling channels, and heat wicking materials.

In the UAM process, a sonotrode driven by a piezoelectric transducer imparts ultrasonic vibrations ($>$ 20 kHz) to a metal foil, creating a scrubbing action and plastic deformation between the foil and the material to which it is being welded (Fig. 1a). The scrubbing action displaces surface oxides, contaminants, and collapses asperities, exposing nascent surfaces that instantaneously bond under a compressive force. Welding a succession of tapes, first side by side and then one top of one another, a three dimensional metal part can be fabricated. By layering foils on top of a "baseplate", UAM can be used as a cladding technology for development of high-value materials over a less expensive substrate. Periodic machining with a built-in CNC stage (Fig. 1b) or laser etching (also incorporated within some UAM systems) allows for selective material removal and in situ machining to final dimensions. The subtractive processes are also utilized to create internal channels for thermal management, to align fibers within the matrix, or for surface texturing of embedded fibers.

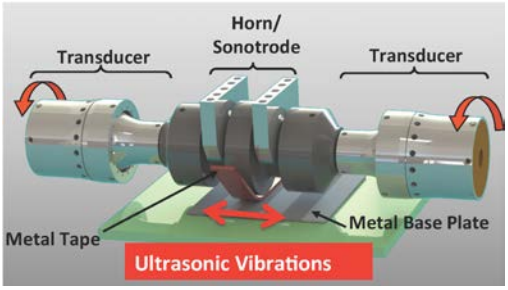

(a)

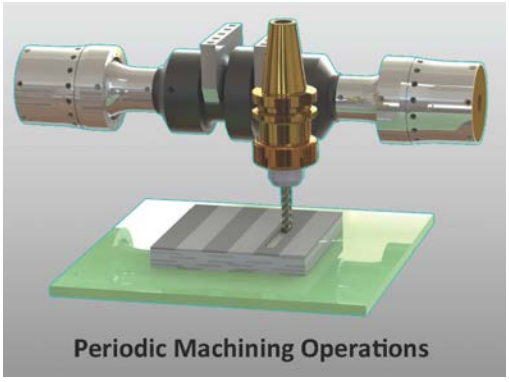

(b)

FIGURE 1. (a) Schematic of a UAM welder, which utilizes ultrasonic vibrations and pressure to join foil stock to a baseplate or other foils. The process is solid state, implying that no fusion is present. (b) The process usually features a CNC mill for conducting subtractive operations.

The most powerful UAM systems currently available deliver 9 kW of ultrasonic power to the weld interface along with higher normal force and high vibration amplitudes. This combination improves the strength and quality of UAM builds, greatly enhances the ability to weld drastically dissimilar materials, and enables previously unfeasible smart structures (Fig. 2). This is illustrated in Fig. 3, where the metallurgical section of an aluminum 3003 build shows gaps left by a low power (1 kW) UAM system, in contrast to a build made with a 9 kW system which shows no gaps despite the material used being harder (aluminum 6061). Even though a low void content does not guarantee high mechanical strength [3], obtaining gapless builds is a necessary condition for optimizing the strength of UAM components [4].

FIGURE 2. New 9 kW, 20 kN UAM system enables joining of dissimilar metals (e.g., structural aluminum, copper, and steels) along with embedded sensors, actuators, and electronic components.

(a) (b)

FIGURE 3. (a) Metallurgical section of aluminum 3003 build showing gaps left by 1 kW UAM system; (b) metallurgical section of gapless aluminum 6061 build fabricated with 9 kW UAM system shown in Fig. 2.

2 EXAMPLE BUILDS AND COMPONENTS

2.1 UAM Galfenol composites for electrically-tunable stiffness structures

Like other magnetostrictive materials, iron-gallium (Galfenol) alloys exhibit a large ΔE effect whereby the elastic modulus increases when the material is magnetized [5]. In combination with Galfenol's high tensile strength and ductility, this property can be used to develop Galfenol structures with magnetically tunable stiffness. The ability to embed Galfenol into aluminum and other metals enables structures with embedded sensing and actuation with the key benefit of protecting the Galfenol elements from corrosive or aqueous environments. Further, the remote activation associated with magnetic fields can be effectively utilized in rotating structures and components that operate in harsh environments.

Galfenol composites are ideally manufactured below the Curie temperature of the material ($\approx 675^{o}$C) to avoid degradation of the material texture and at even lower temperatures ($< 150^{o}$C) to avoid a loss of stress annealing [6]. Schick et al. [7] reported in situ average maximum temperatures below 150^{o}C in aluminum 3003 composites fabricated by UAM. Galfenol wires and thin sheet have been successfully embedded into Al 3003 and Al 6061 structures. Due to the relatively large cross sectional geometry of Galfenol thin sheets, the sheets must be placed in machined grooves prior to subsequent welding of matrix material over top. Representative images of UAM composites containing thin sheets of Galfenol are given in Figure 4.

For functioning smart composites, strain and load transfer at the interface between the active and passive constituents should be maximized. To help determine if metallic bonding of the constituents occurs, energy-dispersive X-ray spectroscopy (EDS) was used to measure the spatial variation in the atomic composition of key elements across the Galfenol-aluminum interface. An example 2-D EDS scan of the interface between Al 3003 and a Galfenol wire is shown in Fig. 4c, where the color intensity indicates the atomic composition. A significant oxide presence at the interface was detected. Further, no evidence of micron-scale diffusion was found. Although this result does not preclude a solid-state weld between the Galfenol fiber and aluminum matrix, it does show that in some cases metallic bonding through micron-scale diffusion is absent at these interfaces. However, as evidenced by Fig. 4b, the UAM process produces intimate contact between the constituents, indicating the presence of strong mechanical interlocking through a friction fit.

Scheidler and Dapino [8] investigated the use of Galfenol/aluminum composite beams operated in clamped-clamped conditions as adaptive vibration absorbers with electrically-tunable stiffness (Figure 5). The resonance frequencies of the beam's first and third bending modes were calculated as a function of DC magnetic field (ranging from 0 to 10 kA/m), base acceleration magnitude (ranging from 0.5 to 20 g), and Galfenol volume fraction (ranging from 10% to 100%). Autoresonant feedback control was used to maintain the resonant state under changes in the inputs; the resonance frequencies were calculated after the autoresonant feedback control stabilized following a change in the inputs. For each Galfenol volume fraction, the resonance frequencies were normalized by the maximum frequency to show the percent change that can be achieved by varying the DC magnetic field. This normalization is consistent with prior work [9]. Results were presented as a series of surfaces (one for each Galfenol volume fraction) using the DC magnetic field and base acceleration limit as independent variables. The data were interpolated to smooth the surfaces. A top view of the surfaces is shown in Figure 6 for the third mode, with results for the first mode being shown to be similar. For Galfenol volume fractions of 82% and 100%, the surfaces are less smooth, because the autoresonant feedback control had difficulty in reaching steady state. This can be attributed to the large spatial and fast temporal variations in the composite's flexural rigidity that occur for these cases.

In all cases, the minimum resonance frequency occurs for small excitation magnitudes and weak magnetic fields, because the flexural rigidity of a Galfenol beam is minimum when stress and magnetic field are small. Weak excitations therefore allow for the greatest change in resonance frequency, because Galfenol can be easily tuned to its stiff (magnetically-saturated) state by

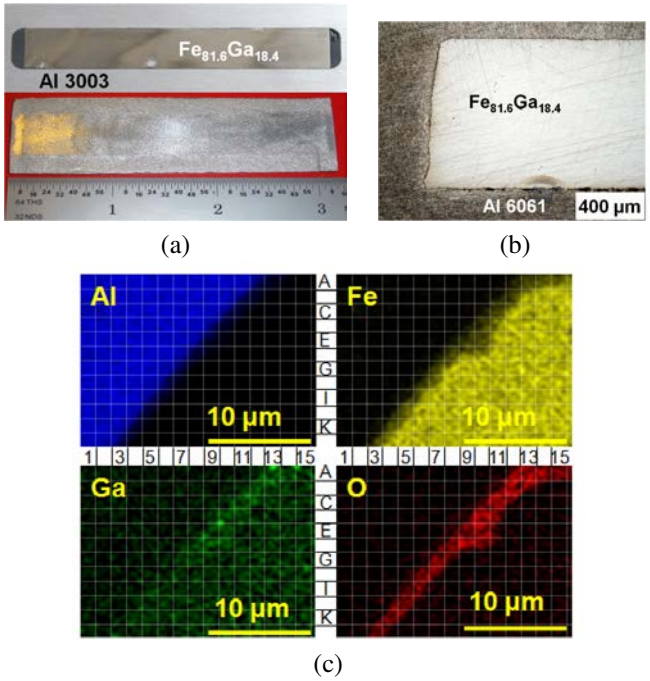

FIGURE 4. (a) Galfenol composite before and after welding, (b) optical microscopy image of a Galfenol composite's cross-section, (c) 2-D EDS scan of the interface between an aluminum matrix and a Galfenol wire embedded in the matrix using UAM.

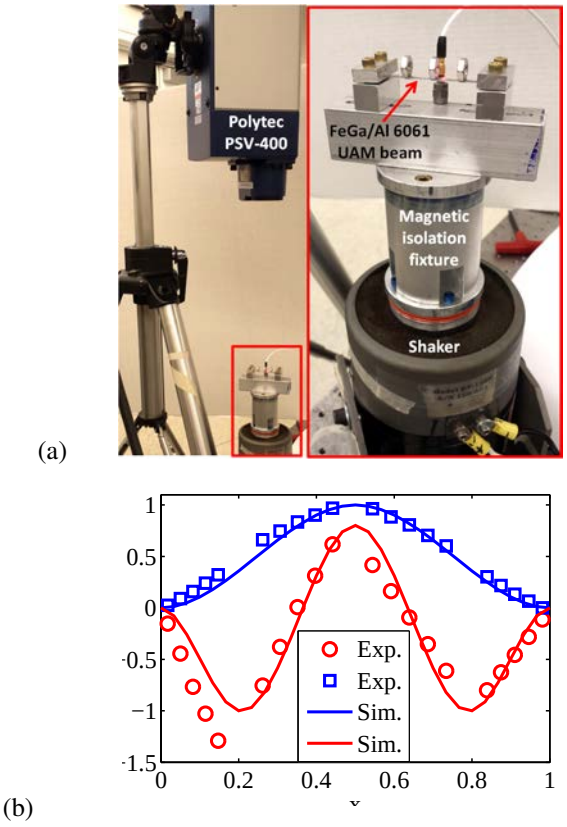

FIGURE 5. (a) Experimental setup for model validation, and (b) experimental and simulated mode shapes of the UAM Galfenol/Al 6061 composite for the first and third modes.

applying stronger DC magnetic fields. As the base acceleration increases, the resulting higher stresses begin to saturate the Galfenol element. Consequently, the composite beam begins to lose its resonant frequency tunability as the Galfenol element behaves like a passive material. These results are supported by previous work [9]. The range of acceleration magnitudes over which the beam's behavior transitions from active to nearly passive will depend on the beam's geometry, the mass loading, and the stiffness of the matrix material. The effect of variations in the elastic modulus of Galfenol on the composite's behavior will be more pronounced for composites with softer matrices. Al 6061 is about 15% to 130% stiffer than Galfenol depending on stress and magnetic field applied to the latter. Thus, in Figure 6, the transition shifts toward smaller accelerations as the Galfenol volume fraction increases.

The compressive axial force generated by applied magnetic fields tends to soften the Galfenol/aluminum beam and reduce its resonance frequencies. This counteracts the stiffening that occurs as the magnetic field tries to saturate the Galfenol element. This is seen in Figure 6 as a broadening of the tunable region along the magnetic field axis. A broadening along the

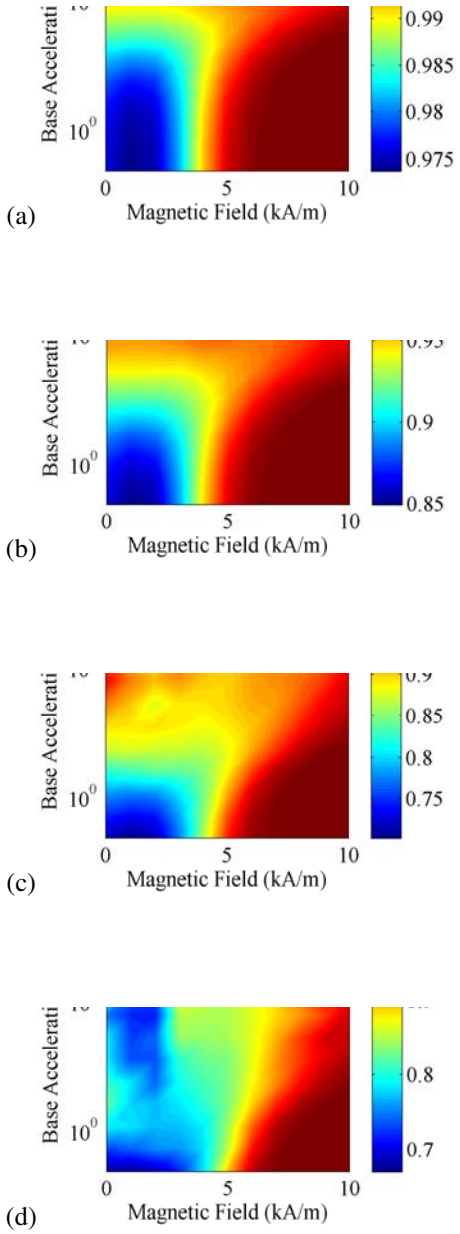

FIGURE 6. Normalized resonance frequency of the third bending vibration mode of a clamped-clamped UAM composite as a function of base acceleration limit and DC magnetic field for Galfenol volume fractions of (a) 10%, (b) 46%, (c) 82%, and (d) 100%.

base acceleration axis was also found for high Galfenol volume fractions. This may be an artifact of the autoresonant feedback control caused by its difficulty in reaching steady state at high volume fractions.

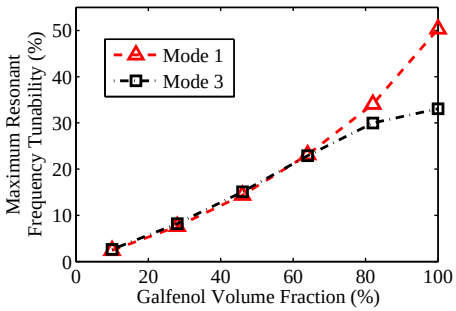

FIGURE 7. Maximum resonance tunability of the Galfenol/Al 6061 beam as a function of Galfenol volume fraction.

A figure of merit for an adaptive vibration absorber is its maximum change in resonance frequency. The dependence of this figure of merit on Galfenol volume fraction is shown in Figure 7 for the first and third modes. The maximum tunability for the first mode increases monotonically from 3% to 51% as Galfenol volume fraction increases from 10% to 100%, respectively. The results for the first mode are very similar to prior work [9], which used a single-degree-of-freedom model and neglected the axial force. Thus, the incorporation of the axial force in this model appears to have only a small effect on the maximum tunability of the first resonance frequency. The maximum tunability of the first and third resonance frequencies was found to be nearly equal except at high Galfenol volume fractions. Thus, with regard to this figure of merit, the performance of the Galfenol beam as an adaptive vibration absorber does not degrade when operated at higher modes.

2.2 SHAPE MEMORY COMPOSITES

Nickel-titanium fibers have been successfully embedded in aluminum matrices utilizing the UAM process. The resulting composites show potential with developing structures with near zero coefficient of thermal expansion (CTE). Evans et al. [10] showed an average CTE of 13 μstrain/degree C (down from 23 μstrain/degree C for aluminum) in NiTI/Al composites in which the SMA serves to restrain the expansion of the Al matrix along the direction of the NiTi fibers. A key advantage of these composites over invar and similar materials is the low density associated with the aluminum matrix. The lighweighting aspect of these composites is crucial for aerospace metering structures. In addition, these composites can potentially utilize the shape memory properties of the SMA as a sensor, actuator, or stiffness tuning device.

Figure 8 shows a metallurgical section of a NiTi ribbon seamlessly embedded in aluminum 3003. More recent work has focused on similar builds with aluminum 6061 [11]. Figure 8 illustrates the intimate contact between the NiTi ribbon and matrix around the entirety of the ribbon perimeter. Top, bottom, and side surfaces as well as corner regions all show close contact even at high magnification. Further, a rough surface can be seen along the NiTi ribbon, indicating that the oxide layer on the ribbon surface has been ruptured creating areas of mechanical interlocking between the ribbon and matrix. There are several visible inclusions in the aluminum matrix. EDS point analyses were conducted on these regions and found consistent compositions of 85.9 at. % Al, 6.8 at. % Mn, and 7.3 at. % Fe, all primary alloying elements in aluminum 3003 [12]. The inclusions are evenly dispersed and as a result appear to be naturally occurring precipitates within the Al tapes and not a result of the UAM process or embedding of the NiTi ribbon.

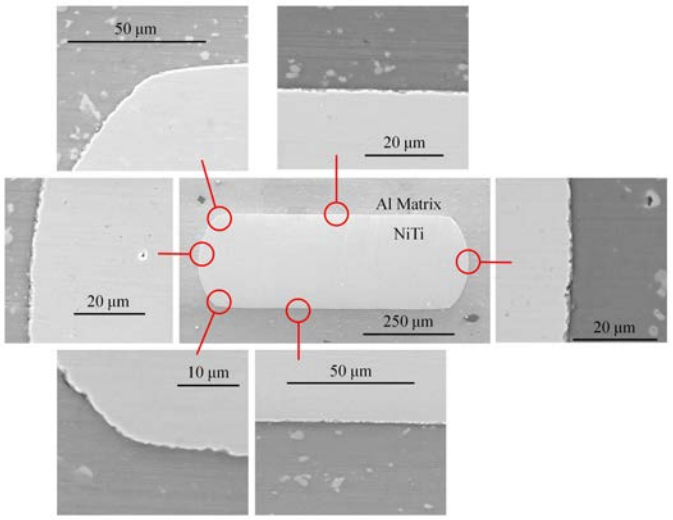

FIGURE 8. SEM image if NiTi-Al 3003 composite showing plastic flow of the matrix enveloping the ribbon and close contact over the entire surface.

Hahnlen [12] conducted differential scanning calorimetry tests on three composites with fully detwinned NiTi ribbons. The results show a consistent interface failure temperature of 68.9 degrees C (Figure 9). The lower transition temperatures observed in the second DSC heating cycle confirm that the embedded NiTi ribbons recovered the induced prestrain in the initial heating cycle and the composites have been irrecoverably changed as a result. Using the models developed by Hahnlen, the blocking stress generated by the NiTi element is estimated to be 176 MPa. Assuming a friction dominated interface, the ultimate shear strength of the NiTi-Al interface is determined to be 7.36 MPa. While the interfacial shear strength and the blocking force are not dependent upon length of the embedded NiTi elements, the shear stress at the interface is inversely proportional to ribbon length. This suggests that by increasing the composite length the interface failure temperature is increased significantly, avoiding ir-

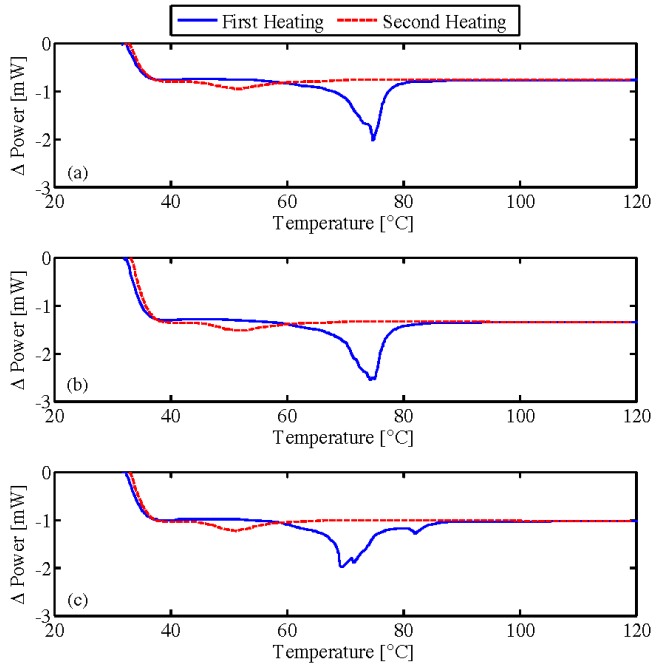

FIGURE 9. DSC results for three samples of a given composite build.

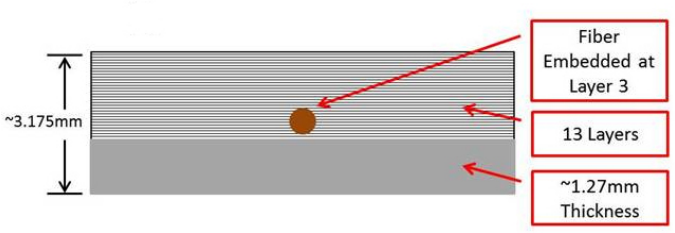

FIGURE 10. Schematic of sample cross section with key fabrication details.

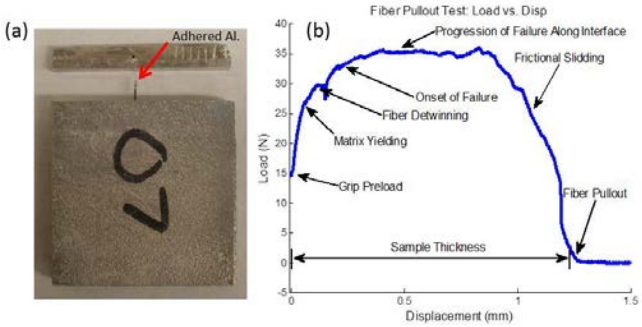

FIGURE 11. Representative pullout test result for oxide layer sample: (a) photo of sample after failure illustrating adhered aluminum to surface of fiber; (b) detailed force-displacement pullout test curve.

recoverable composite damage. Ultimately, composite failure may not be limited by interface strength, but instead by material yield strengths and critical buckling loads.

Hehr et al. [11] further investigated the interfacial shear strength of NiTi/Al composites made by ultrasonic additive manufacturing. Using single fiber pull out tests, they found that the matrix yielded prior to the interface breaking since adhered aluminum was consistently observed on all pullout samples. The sample design is shown in Figure 10. Aluminum 6061-O fully work hardened foil was utilized as the metal matrix for the NiTi-Al UAM composite. The NiTi fiber diameter was 0.28 mm (0.011") as supplied from Nitinol Devices & Components, Inc., in four different surface finishes (regular oxide layer, mechanically roughened, chemically etched, and mechanically polished). All of the material was trained straight for it to be superelastic. A representative fiber pullout force-displacement curve and tested oxide surface finish sample can be seen in Figure 11.

SEM images of sample cross sections for each surface finish are shown in Figure 12. These samples were not used in mechanical testing, but were made separately with the same welding conditions as the pullout samples. Tape interfaces cannot be identified easily, which illustrates the consolidation effectiveness of the 9 kW UAM system. Additionally, the Al 6061-T6 base plate material can be identified as the area with the slight contrast difference directly below the fiber. Finally, it can be seen that all the fibers were encapsulated well with some void character. Unexpectedly, some of these voids occur near the bottom of the fiber in the oxide and chemically etched surface finishes compared to the top of the fiber, like the mechanically polished finish. This odd bottom of pocket void characteristic could have originated from contaminants on the fiber surface prior to consolidation, which could limit bonding around the fiber, or the contaminants could promote a corrosive reaction with a chemical utilized in the polishing process.

A finite element model was developed within COMSOL to emulate fiber pullout test conditions on the fiber pullout sample. The calculations show that deformation of the samples is highly localized around the fiber, as desired, to minimize unwanted bending loads. The calculated average peak shear stress was shown to be independent of the sample length, which, in turn, correlates well with consistently observed failure loads for all samples and smearing of the average shear stress for longer sample lengths. The average peak shear stress is near or above the ultimate shear strength of the Al tapes utilized in the UAM process, which explains the reason for the matrix failing and leaving an aluminum residue on pulled out fibers (Figure 11(a)). The calculations suggest that the Al matrix experienced a peak shear stress near 230 MPa, which is higher than the ultimate shear strength of 150-200 MPa for aluminum. This result is in line with the matrix

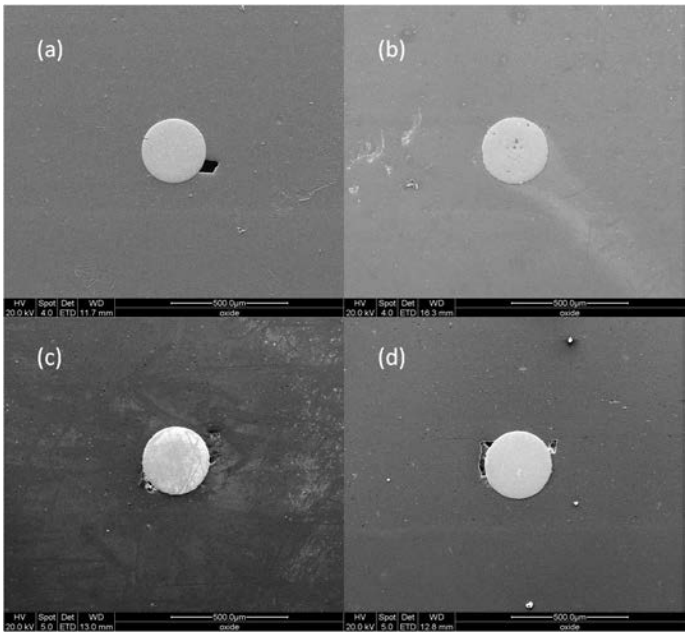

FIGURE 12. SEM images of embedded NiTi fibers utilized by Hehr et al. [11]: (a) oxide surface finish; (b) mechanically roughened surface finish; (c) chemically etched surface finish; (d) mechanically polished surface finish

failure observed during testing. Consequently, bond mechanisms for all fiber surface finishes supersede the strength of the Al matrix and show that there is no clear optimal surface finish. However, with the use of stronger Al matrices or characterization of the interface at elevated temperatures, surface finish may play a larger role in failure.

2.3 UAM FOR THERMAL MANAGEMENT

The need to extract or supply heat at certain locations in a structure is a key requirement for many engineering systems. This is often accomplished by placing heat sinks on the exterior of the structure near the heat source. A more effective approach is to design the structure with internal channels at the source and pump fluid through the channels. The conventional methods for manufacturing such structures are casting and extrusion. Common problems with casting include the formation of inclusions, oxides, and second phases, porosity, and a variation in the microstructure (and therefore material properties) of parts with nonuniform cooling rates [13]. Further, the casting of multimaterial components is usually impractical due to the formation of brittle intermetallics and differences in cooling behavior. Cold and hot extrusion also cannot directly manufacture multimaterial components. Additionally, the complexity of extruded shapes is limited and parts must have a constant cross-section [14]; thus, only straight internal channels are possible. To realize advanced thermal management designs that utilize conformal cooling and heating channels, additive manufacturing technologies can be employed. Of these technologies, UAM is well suited for the manufacture of complex parts due to the ability of the process to weld dissimilar materials and embed components such as cooling tubes or heat wicking materials (Figure 13).

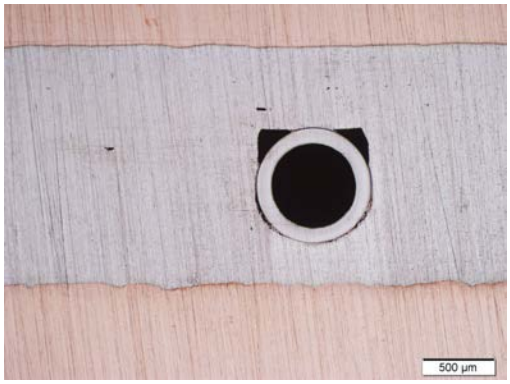

FIGURE 13. Cross section of a UAM build including copper, aluminum, and a cooling channel.

Figure 14 shows a table top demonstrator of a UAM cooling system. The system consists of two blocks manufactured using UAM that each contain straight and block O-shaped internal channels (as shown by the x-ray image). One block is heated by a cartridge heater inserted below the channels to simulate a heat source. The block is actively cooled by flowing water pumped through a closed circuit. The water also flows through the second UAM block, which is cooled by thermoelectric modules to extract heat from the fluid and allow for continuous cooling of the heated block. When powered, the cartridge heater generates a steady-state temperature of 108 degrees C in the heated block. When the pump is turned on, the temperature drops to to 49 degrees C in less than a minute. Commercial parts can also incorporate 3-D channels or functional grading of materials, which seamlessly integrates economical materials with high-value, heat-wicking materials to simultaneously optimize performance and cost or strength.

3 CONCLUDING REMARKS

Ultrasonic additive manufacturing is a solid-state manufacturing process that allows the fabrication of structures with dissimilar metals and embedded features such as smart materials, cooling devices, and electronics. A critical advantage of UAM of low process temperatures implies that the process does not degrade the properties of the smart materials being embedded. This paper discussed three UAM builds including Galfenol beams for

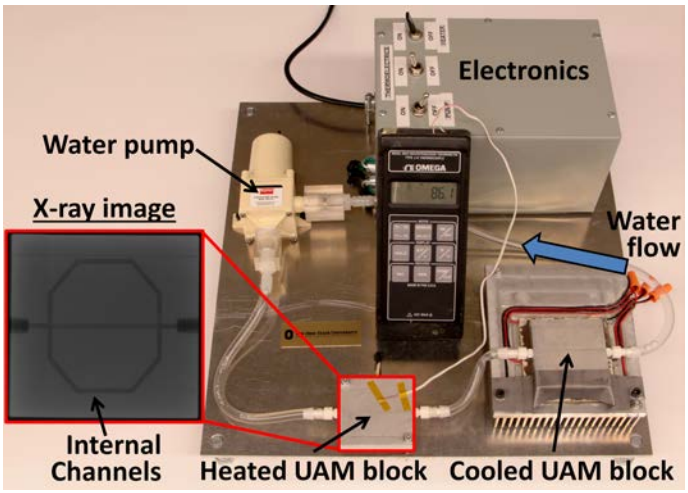

FIGURE 14. Thermal management demonstrator.

adaptive vibration absorbers, NiTi/Al composites for zero CTE applications, and structures with embedded cooling channels.

ACKNOWLEDGEMENTS

Support comes from Ohio Department of Development, Third Frontier Project # TECH 12-067, and from the member organizations of the Smart Vehicle Concepts Center (www.SmartVehicleCenter.org), a National Science Foundation Industry/University Cooperative Research Center.

REFERENCES

[1] Wohlers Report, http://wohlersassociates.com/2013report.htm, 2013.

[2] K.F. Graff, Ultrasonic Additive Manufacturing, *Welding Fundamentals and Processes*, ASM Handbook, Vol, 6A, 2011.

[3] C. Hopkins, P. J. Wolcott, M. J. Dapino, A. C. Truog, S. S. Babu, Optimizing ultrasonic additive manufactured Al 3003 properties with statistical modeling, *J. Eng. Mater. Technol.*, Vol. 134, Issue 1, p. 011004, 2012.

[4] C.D. Hopkins, M.J. Dapino, and S.A. Fernandez, Statistical characterization of Ultrasonic Additive Manufacturing Ti/Al composites, *ASME Journal of Engineering Materials and Technology*, Vol. 132, Issue 4, 041006, October 2010.

[5] S. Datta, J. Atulasimha, C. Mudivarthi, A.B. Flatau, "Stress and magnetic field-dependent Young's modulus in single crystal iron–gallium alloys," *Journal of Magnetism and Magnetic Materials,* Vol. 322, Issue 15, pp. 2135-2144, 2010.

[6] J. Atulasimha and A.B. Flatau, "A review of magnetostrictive iron–gallium alloys," *Smart Materials and Structures,* Vol. 20, Issue 4, p. 043001, 2011.

[7] D. Schick, S.S. Babu, D.R. Foster, M.J. Dapino, M. Short, and J.C. Lippold, "Transient thermal response in ultrasonic additive manufacturing of aluminum 3003," Vol. 17, Issue 5, pp. 369-379, 2011.

[8] J. Scheidler and M.J. Dapino, "Nonlinear dynamic model for magnetically-tunable Galfenol vibration absorbers," Proc. SPIE Smart Materials and Structures & Structural Health Monitoring, San Diego, CA, March 2014.

[9] J.J. Scheidler and M.J. Dapino, "Nonlinear dynamic modeling and resonance tuning of Galfenol vibration absorbers," *Smart Materials and Structures*, Vol. 22, Issue 8, p. 085015, 2013.

[10] P.G. Evans, J. Pritchard, R. Hahnlen, and M.J. Dapino, "Dimensionally stable optical metering structures with NiTi composites fabricated through ultrasonic additive manufacturing," Prof. ASME SMASIS Conference on Smart Materials, Adaptive Structures and Intelligent, SMASIS2013-3204, Snowbird, Utah.

[11] A. Hehr, J. Pritchard, and M.J. Dapino, "Interfacial shear strength estimates of NiTi-Al matrix composites fabricated via ultrasonic additive manufacturing," Proc. SPIE Smart Materials and Structures & Structural Health Monitoring, San Diego, CA, March 2014.

[12] R. Hahnlen, "Characterization and modeling of active metal-matrix composites with embedded shape memory alloys," Ph.D. Dissertation, The Ohio State University, Columbus, Ohio, 2012.

[13] , ASM Handbook, Vol. 20: Materials Selection and Design, ASM International, CRC Press, 1997.

[14] ASM Handbook, Vol. 14A: Metalworking: Bulk Forming, ASM International, CRC Press, 1997.